

Alloy Engineering of Topological Semimetal Phase Transition in $\text{MgTa}_{2-x}\text{Nb}_x\text{N}_3$

Huaqing Huang,¹ Kyung-Hwan Jin,¹ and Feng Liu^{1,2,*}

¹*Department of Materials Science and Engineering, University of Utah, Salt Lake City, Utah 84112, USA*

²*Collaborative Innovation Center of Quantum Matter, Beijing 100084, China*



(Received 28 November 2017; published 27 March 2018)

Dirac, triple-point, and Weyl fermions represent three topological semimetal phases, characterized with a descending degree of band degeneracy, which have been realized separately in specific crystalline materials with different lattice symmetries. Here we demonstrate an alloy engineering approach to realize all three types of fermions in one single material system of $\text{MgTa}_{2-x}\text{Nb}_x\text{N}_3$. Based on symmetry analysis and first-principles calculations, we map out a phase diagram of topological order in the parameter space of alloy concentration and crystalline symmetry, where the intrinsic MgTa_2N_3 with the highest symmetry hosts the Dirac semimetal phase, which transforms into the triple-point and then the Weyl semimetal phases with increasing Nb concentration that lowers the crystalline symmetries. Therefore, alloy engineering affords a unique approach for the experimental investigation of topological transitions of semimetallic phases manifesting different fermionic behaviors.

DOI: 10.1103/PhysRevLett.120.136403

Alloying engineering is one of the most well-established approaches to tailor a material's structural, mechanical, and electronic properties [1,2]. For example, the classical Vegard's law underlies the fact that the lattice constant of an alloy $A_{1-x}B_x$ is usually a linear interpolation of the lattice constants of A and B [3,4]. The well-known bowing curve provides a useful guideline for determining the band gap of a semiconductor alloy [5–7]. Recently, alloy engineering has also been extended to tailor the topological material properties [8–13], such as the Fermi energy, spin chirality, Fermi arcs, and the phase transition between trivial and topological states. In this Letter, we demonstrate for the first time that alloy engineering can also be applied to tune the transitions among different topological fermions in topological semimetals.

Topologically protected fermionic quasiparticles in semimetals are directly related to the degeneracy of band crossing points around the Fermi level, which are determined by the crystalline symmetry. Fourfold Dirac fermions in Dirac semimetals, such as Na_3Bi [14] and Cd_3As_2 [15], are protected by inversion, time-reversal, and rotational symmetries. Weyl fermions with twofold degeneracy are observed in Weyl semimetals with broken inversion [16–18] or time-reversal symmetry [19]. Triple-point fermions, an intermediate state between fourfold Dirac and twofold Weyl fermions, can be realized in noncentrosymmetric tungsten carbide-type materials with certain crystalline symmetries [20–22]. Although different fermions are realized in different crystal materials with specific lattice symmetry, few of them can exist in a single material simultaneously [23–26]. It is well known that a Dirac fermion would split into a pair of Weyl fermions by breaking either the inversion or time-reversal symmetry of a Dirac semimetal [14,27,28]. Actually, it is theoretically possible to realize all these fermions by

gradually reducing the crystalline symmetry of certain compounds. However, such three-stage transition in a real material has never been seen yet; also, the study of coexistence and interplay between these fermions is still lacking. Hence, realizing the transition between Dirac, triple-point, and Weyl fermionic quasiparticles in one single material system is of great importance for material science, condensed matter physics, and elementary particle physics.

Here, we propose an alloy engineering approach to realize all three types of fermions in a single material system. Taking $\text{MgTa}_{2-x}\text{Nb}_x\text{N}_3$ as an example, we show that Dirac fermions which exist in the intrinsic MgTa_2N_3 with the highest symmetry can be converted into triple-point and Weyl fermions with increasing Nb concentration that lowers the crystalline symmetries. The evolution of Fermi arcs and quasiparticle interference (QPI) spectra in different topological semimetallic states have been studied in depth. Our findings not only are of fundamental interest for a better understanding of basic properties of different topological fermions but also provide a unique approach for the experimental investigation of phase transitions among different topological states.

We performed first-principles calculations for $\text{MgTa}_{2-x}\text{Nb}_x\text{N}_3$ using the Vienna *ab initio* simulation package [29]. Details of computational methods are presented in the Supplemental Material [30]. MgTa_2N_3 , which has already been synthesized [66], crystallizes in a hexagonal crystal structure with space group $P6_3/mcm$ (D_{6h}^3 , No. 193), as shown in Fig. 1(a). In this structure, Mg/Ta layers are sandwiched by N layers alternatively. Every Mg atom lies in the center of an octahedron of N atoms. Ta atoms are divided into two groups: δ - and θ -Ta. The δ -Ta atoms, which are in the Mg layer, occupy the centers of octahedra, similar to the case

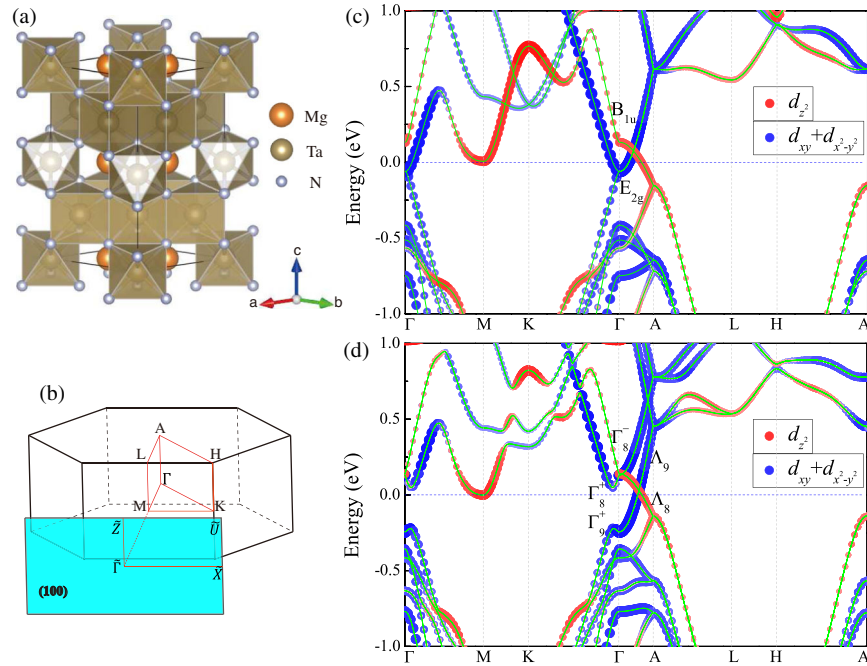


FIG. 1. (a) Crystal structure of MgTa_2N_3 with $P6_3/mcm$ (No. 193) symmetry in a hexagonal cell. (b) The Brillouin zone of MgTa_2N_3 and the projected surface Brillouin zones of the (100) surface. Band structure of MgTa_2N_3 (c) without SOC and (d) with SOC. Red and blue dots in band structures indicate the projection onto the Ta d_{z^2} and $d_{xy} + d_{x^2-y^2}$ orbitals, respectively.

in δ -TaN [67], whereas θ -Ta atoms lie in the adjacent plane and are located in the centers of pentahedra of N atoms, similar to the case in θ -TaN [68]. The calculated lattice constants are $a = 5.218 \text{ \AA}$ and $c = 10.435 \text{ \AA}$, consistent with the experimental values [66].

Figure 1(c) shows the band structure of MgTa_2N_3 without considering spin-orbit coupling (SOC). Apparently, MgTa_2N_3 is a metal with both electron and hole pockets at the Fermi level, and there is a band crossing along Γ -A due to the band inversion between the B_{1u} and E_{2g} states at Γ . The orbital-resolved bands clearly show that the crossing bands consist of one band composed of the Ta d_{z^2} orbital and one double-degenerate band derived from the $d_{x^2-y^2}$ and d_{xy} orbitals. Because these two crossing bands belong to different irreducible representations of the C_{3v} symmetry group of Γ -A, the band crossing point is threefold (or sixfold if the spin degree of freedom is considered) degenerate and protected by the C_{3v} rotational symmetry. This would suggest that MgTa_2N_3 were a triple-point semimetal without considering SOC. However, since Ta is a heavy element with strong SOC, we further calculated the band structure in the presence of SOC, as shown in Fig. 1(d). The $d_{x^2-y^2}$ - and d_{xy} -dominated E_{2g} state splits into Γ_8^+ and Γ_9^+ states with $J_z = \pm 1/2$ and $\pm 3/2$, respectively (J_z is the total angular momentum), while the d_{z^2} -derived B_{1u} state becomes the Γ_8^- state with $J_z = \pm 1/2$. Since both time-reversal and inversion symmetries are present, every band is spin degenerate. Duo to the C_{3v} symmetry, the Λ_8 and Λ_9 bands with different irreducible

representations cannot hybridize with each other [30]. This leads to a symmetry-protected fourfold-degenerate band-crossing point along Γ -A. Hence, the system is actually a three-dimensional (3D) Dirac semimetal with a pair of Dirac points at $(0, 0, k_z^D = \pm 0.293)$ (in units of $2\pi/c$) with an energy of $E_D = 29 \text{ meV}$ above the Fermi level due to the small electron pocket around M . We also calculated the Fermi velocity of the Dirac cone ($v_x = 2.07, v_y = 2.08, v_z^{+/-} = 2.87/1.11$) eV \AA , which is comparable with that of the typical Dirac semimetal Na_3Bi [14]. Different from the case of Na_3Bi , the Dirac cone in MgTa_2N_3 is more isotropic but tilts slightly along the k_z direction. Moreover, the Dirac cone is mainly composed of d orbitals pertaining to the investigation of the strong correlation effect or magnetism in d -electron-mediated Dirac fermion systems [69].

Subsequently, we studied the alloying effect in $\text{MgTa}_{2-x}\text{Nb}_x\text{N}_3$ by the virtual crystal approximation (VCA) [70]. The VCA treatment typically gives a reasonable description for solid-solution systems in which the dopant and host atoms have a similar chemical character. As shown in Fig. 2(a), with a varying concentration of Nb, the energy splitting between Γ_8^+ and Γ_9^+ decreases linearly. This is because the SOC strength of Nb is much weaker, so that the SOC-induced splitting becomes smaller with increasing Nb alloying concentration. Meanwhile, the band crossing points gradually move away from the Fermi level. We also calculated the topological invariants for different concentrations. Although Nb alloying changes the electronic structures around the Fermi level, the nontrivial band topology remains, as discussed later.

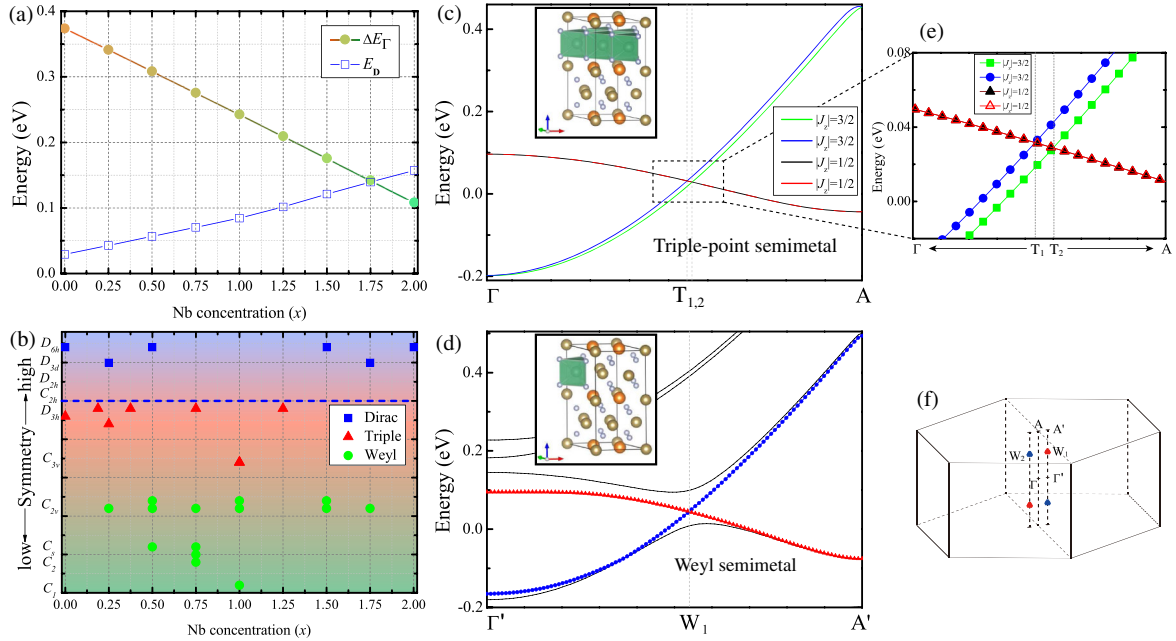


FIG. 2. (a) Energy splitting between Γ_8^+ and Γ_9^+ states (ΔE_{Γ}) and the energy of the Dirac point (E_D) in $\text{MgTa}_{2-x}\text{Nb}_x\text{N}_3$ under the VCA. (b) Symmetry-breaking effect of Nb doping using the supercell simulation. Each point represents a configuration with different symmetry. Band structures of example configurations that host (c) triple-point [$\text{MgTa}_{1.25}\text{Nb}_{0.75}\text{N}_3$ (D_{3h})] and (d) Weyl semimetal states [$\text{MgTa}_{1.75}\text{Nb}_{0.25}\text{N}_3$ (C_{2v})]. The insets show the corresponding atomic configurations. (e) The zoomed-in plot of band structures around the triple points. (f) Schematic illustration of the Weyl point distribution in the 3D Brillouin zone where red and blue dots represent Weyl points with a Chern number of -1 or $+1$.

As the VCA method only gives an average effect without accounting for local inhomogeneity, we further adopted supercell simulations to investigate the effect of symmetry breaking induced by different local atomic environments in the alloyed $\text{MgTa}_{2-x}\text{Nb}_x\text{N}_3$. We studied about 40 configurations with different symmetry groups, alloying concentrations, and supercell sizes (see Supplemental Material [30]). The results are presented in Fig. 2(b). Interestingly, we found that by breaking inversion symmetry while keeping some crystalline symmetries (e.g., C_{3v}), a fourfold Dirac point splits into a pair of triply degenerate points along the k_z axis. Further reducing the crystalline symmetries, the triple points become Weyl points departing from the k_z axis. As examples of triple-point and Weyl semimetals, below we present detailed results for two configurations with different symmetries and alloying concentrations: $\text{MgTa}_{1.25}\text{Nb}_{0.75}\text{N}_3$ (D_{3h}) and $\text{MgTa}_{1.75}\text{Nb}_{0.25}\text{N}_3$ (C_{2v}).

The band structures of the triple-point semimetal are shown in Figs. 2(c) and 2(e). Because the D_{3h} crystalline symmetry of the alloyed system includes C_{3v} but excludes inversion symmetry, two $|J_z| = 3/2$ bands split gradually along Γ -A and cross with the doubly degenerate $|J_z| = 1/2$ bands, forming two pairs of triply degenerate points at $(0, 0, k_z^{T_1} = \pm 0.267)$ and $(0, 0, k_z^{T_2} = \pm 0.273)$ (in units of $2\pi/c$), respectively, with an energy difference of

$\Delta E^T = 2.86$ meV. Unlike other candidate semimetals with multiple pairs of triple points [20–22], this system exhibits a minimal number of triple points as required by time-reversal symmetry, which provides an “ideal” base system to study the properties solely induced by triple-point fermions [71]. This selectively Nb-alloyed $\text{MgTa}_{2-x}\text{Nb}_x\text{N}_3$ is expected to be grown by molecular beam epitaxy techniques, which have been proven to be an atomically accurate growth method for high-quality samples, such as modulation-doped $\text{Ga}_{1-x}\text{Al}_x\text{As}/\text{GaAs}$ superlattices [72,73], doped III-V nitrides [74,75], and topological-insulator alloys $(\text{Bi}_{1-x}\text{Sb}_x)_2\text{Te}_3$ [76]. The experimental feasibility of synthesizing and growing the $\text{MgTa}_{2-x}\text{Nb}_x\text{N}_3$ alloys is discussed in detail in the Supplemental Material [30]. Interestingly, we also found that breaking symmetries by substitutional alloying cannot drive the p -electron Dirac fermion in Na_3Bi into triple-point fermions [9,30], indicating that our finding might be a unique feature of d -electron-media Dirac fermions, such as the case in MgTa_2N_3 .

The Weyl semimetal state is obtained by further reducing the crystalline symmetry. As shown in Fig. 2(d), two nondegenerate bands cross each other along Γ' -A', which is slightly away from the Γ -A line. This leads to the formation of Weyl points at $(0.00779, -0.0003, \pm 0.269)$ and $(-0.00749, 0.0003, \pm 0.269)$ [in units of $(2\pi/a, 2\pi/a, 2\pi/c)$] that are related by time-reversal and C_{2v} symmetries

[see Fig. 2(f)]. The average Wannier charge centers are calculated by the Wilson-loop method on the sphere enclosing the Weyl point, from which the Chern number ($-1/+1$) of each pair of Weyl points (W_1/W_2) is obtained (see Supplemental Material [30]). Note that this system exhibits only two pairs of Weyl points—the minimum number possible in time-reversal-invariant systems, which provides an “ideal” platform for studying exotic properties of Weyl fermions in experiments.

To further reveal the transition from Dirac to triple-point fermions in the alloyed $\text{MgTa}_{2-x}\text{Nb}_x\text{N}_3$, we constructed a low-energy effective Hamiltonian using the method of invariants [77]. Due to the C_3 rotation and inversion symmetries of the system, it is more convenient to make a linear combination of the Ta d_{z^2} , $d_{x^2-y^2}$ and d_{xy} orbitals as $d_{\pm 2} = d_{x^2-y^2} \pm id_{xy}$, which have the z -direction orbital angular momentum $L_z = \pm 2$. By including SOC in the hybridized orbital picture, the d_{z^2} orbital contains two states with $J_z = \pm \frac{1}{2}$, which compose the Λ_8 band, while the two $d_{\pm 2}$ orbitals become four states with $J_z = \pm \frac{1}{2}, \pm \frac{3}{2}$, which contribute to the two SOC-split bands. Using the Γ_8^- and Γ_9^+ states as a basis, we can then derive an effective 4×4 Hamiltonian by considering the time-reversal and D_{3h}^3 symmetries:

$$H_{\text{eff}}(\mathbf{k}) = \begin{pmatrix} \epsilon_1(\mathbf{k}) & 0 & Ak_+ & 0 \\ 0 & \epsilon_1(\mathbf{k}) & 0 & -Ak_- \\ Ak_- & 0 & \epsilon_2(\mathbf{k}) & D(\mathbf{k}) \\ 0 & -Ak_+ & D^*(\mathbf{k}) & \epsilon_2(\mathbf{k}) \end{pmatrix},$$

where $\epsilon_j(\mathbf{k}) = E_j + F_j k_z^2 + G_j(k_x^2 + k_y^2)$ ($j = 1, 2$) and $k_{\pm} = k_x \pm ik_y$. The term $D(\mathbf{k})$ describes the breaking of inversion symmetry, which should be zero for intrinsic MgTa_2N_3 . The material-dependent parameters in the above Hamiltonian are determined by fitting the energy spectrum of the effective Hamiltonian to that of first-principles calculations. Defining $M(\mathbf{k}) = \epsilon_1(\mathbf{k}) - \epsilon_2(\mathbf{k}) = M_0 - M_1 k_z^2 - M_2(k_x^2 + k_y^2)$, we obtained the eigenvalues of the above Hamiltonian $E(\mathbf{k}) = \frac{1}{2}[\epsilon_1(\mathbf{k}) + \epsilon_2(\mathbf{k}) \pm \sqrt{M(\mathbf{k})^2 + 4A^2 k_+ k_-}]$ and found two gapless solutions at $\mathbf{k}^D = [0, 0, k_z^D = \pm \sqrt{(M_0/M_1)}]$, which are nothing but the Dirac points discussed above. For the triple-point semimetal state in the alloyed $\text{MgTa}_{2-x}\text{Nb}_x\text{N}_3$ with D_{3h} symmetry, the inversion-breaking term $D(\mathbf{k}) = D_1 k_z$ is no longer vanishing. It is straightforward to derive that the triple points are $\mathbf{k}^T = [0, 0, k_z^T = \pm \sqrt{(M_0/M_1) + (|D_1|^2/4M_1^2)} \mp (|D_1|/2M_1)] \approx \pm k_z^D \pm (|D_1|/2M_1)$, indicating that each Dirac point splits into a pair of triple points in the k_z axis.

To confirm the nontrivial topological nature of MgTa_2N_3 , we calculated the \mathbb{Z}_2 topological invariants by directly tracing the evolution of 1D hybrid Wannier charge centers [78] during a “time-reversal pumping”

process as proposed by Soluyanov and Vanderbilt [79]. Although MgTa_2N_3 is a semimetal without a global gap, the electronic structures within the $k_z = 0$ and $k_z = \pi$ planes are fully gapped; hence, \mathbb{Z}_2 topological invariants are well defined in these planes and can be used to identify the band topology. Opposite to the case of Na_3Bi [14], it is found that $\mathbb{Z}_2 = 1$ for the $k_z = 0$ plane, whereas $\mathbb{Z}_2 = 0$ for the $k_z = \pi$ plane in MgTa_2N_3 . Therefore, a band inversion between the Λ_9 and Λ_8 bands should occur along the k_z direction as seen above [see Fig. 1(d)]. Consequently, MgTa_2N_3 is a topologically nontrivial 3D Dirac semimetal with topological surface states and Fermi arcs appearing on its side surfaces. It is worth noting that the above calculation of a topological invariant is also valid for the alloyed $\text{MgTa}_{2-x}\text{Nb}_x\text{N}_3$, which indicates that topological surface states also exist on the surfaces of triple-point and Weyl semimetal phases of the $\text{MgTa}_{2-x}\text{Nb}_x\text{N}_3$ alloy. We calculated the \mathbb{Z}_2 topological invariants of two representative configurations discussed above, confirming the nontrivial topological nature of triple-point and Weyl semimetal phases of $\text{MgTa}_{2-x}\text{Nb}_x\text{N}_3$. (see Supplemental Material [30]).

In Fig. 3, we present the (100) surface states of $\text{MgTa}_{2-x}\text{Nb}_x\text{N}_3$ that host Dirac, triple, and Weyl semimetal states, respectively. Since the $k_z = 0$ and $k_z = \pi$ planes have different \mathbb{Z}_2 invariants for all topological semimetals in the $\text{MgTa}_{2-x}\text{Nb}_x\text{N}_3$ alloy, the number of surface states is odd and even along the $\tilde{\Gamma}-\tilde{X}$ and $\tilde{Z}-\tilde{U}$ lines of the surface BZ, respectively, for all cases in Fig. 3. For the Dirac semimetal, the surface state on the k_z axis is twofold degenerate [30]. Hence, two pieces of Fermi arcs stick together at two singularity points where the surface projections of bulk Dirac points appear, as shown in Fig. 3(a). In the triple-point semimetal, the Dirac point splits into two triple points along the k_z axis, each of which contributes a nondegenerate surface state. Hence, the Fermi arcs are gapped in the k_z axis, and an extra Fermi arc crosses the boundary of the surface Brillouin zone to connect two Fermi pockets containing the projected triple points [see Fig. 3(b)]. In the Weyl semimetal, because a Dirac point splits into a pair of Weyl points with opposite Chern numbers, two Fermi arcs connecting the projected Weyl points split also and locate in the opposite sides of the k_z axis [see Fig. 3(c)]. Having the Fermi arcs of different topological semimetals which can be measured by angle-resolved photoemission spectroscopy techniques, we further analyzed their fingerprints in QPI spectra [30], which can be observed by scanning tunneling spectroscopy (STS) measurements [80–83]. As shown in Figs. 3(d)–3(f), both Dirac and Weyl semimetals exhibit a stripe-type STS pattern, whereas the triple-point semimetal shows a flower-shaped STS pattern with four petals due to the extra Fermi arc across the boundary of the surface Brillouin zone. The QPI spectra reveal the scattering processes of surface states by defects, which are broadly relevant to

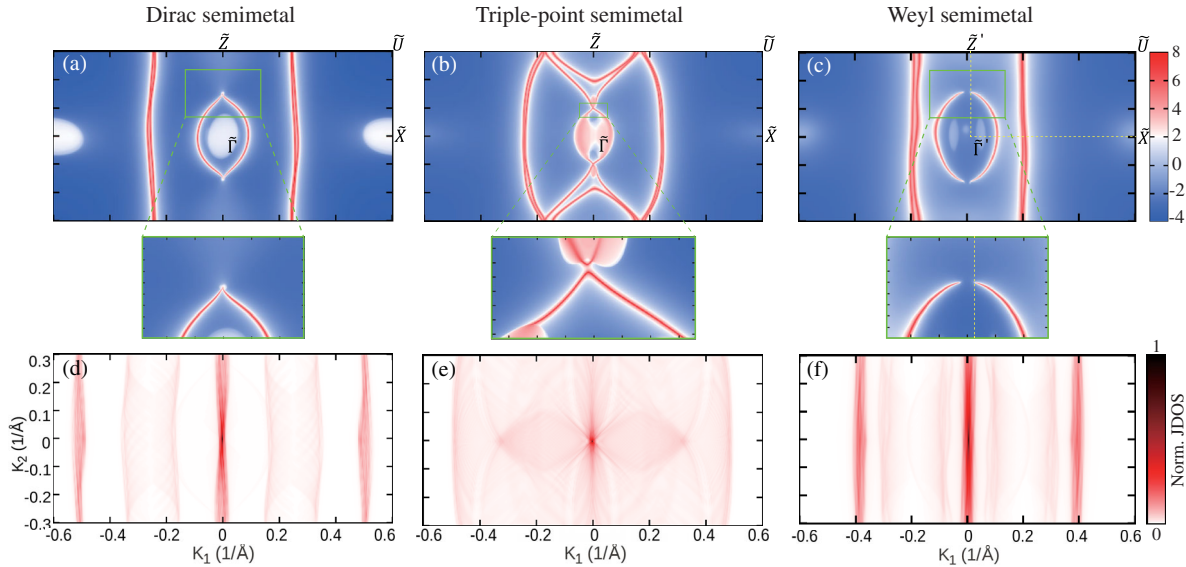


FIG. 3. The projected isoenergy surface and QPI pattern for the (100) surface of $\text{MgTa}_{2-x}\text{Nb}_x\text{N}_3$. (a) and (d): The Fermi arc and QPI pattern at E_D of the Dirac semimetal (MgTa_2N_3). (b) and (e): The Fermi surface and QPI pattern around the band crossings of the triple-point semimetal [$\text{MgTa}_{1.25}\text{Nb}_{0.75}\text{N}_3$ (D_{3h})]. (c) and (f): The Fermi arc and QPI pattern at the energy of Weyl point E_W of the Weyl semimetal [$\text{MgTa}_{1.75}\text{Nb}_{0.25}\text{N}_3$ (C_{2v})]. The QPI patterns are derived from the surface-state-based calculations.

surface transport and device application based on these topological semimetals.

In conclusion, we significantly expand the horizon of a classical materials engineering approach, alloy engineering, to a new territory for realizing different fermions in one single material system. This is exemplified by calculating the phase transitions among Dirac, triple-point, and Weyl semimetal states in the $\text{MgTa}_{2-x}\text{Nb}_x\text{N}_3$ system. Our finding provides useful guidance for designing topological semimetallic materials that can host different fermionic quasiparticles. Our proposed approach of engineering topological states by alloying is general, not only applicable to other 3D topological fermions but also extendable to 2D topological surface fermions [84,85] via surface alloying [86–88].

This work was supported by U.S. DOE-BES (Grant No. DE-FG02-04ER46148). The calculations were done on the CHPC at the University of Utah and DOE-NERSC.

*Corresponding author.
fliu@eng.utah.edu

- [1] W. Pfeiler, *Alloy Physics: A Comprehensive Reference* (John Wiley & Sons, New York, 2008).
- [2] A.-B. Chen and A. Sher, *Semiconductor Alloys: Physics and Materials Engineering* (Springer Science & Business Media, New York, 2012).
- [3] L. Vegard, *Z. Phys.* **5**, 17 (1921).
- [4] A. R. Denton and N. W. Ashcroft, *Phys. Rev. A* **43**, 3161 (1991).
- [5] J. A. Van Vechten and T. K. Bergstresser, *Phys. Rev. B* **1**, 3351 (1970).

- [6] A. Zunger and J. E. Jaffe, *Phys. Rev. Lett.* **51**, 662 (1983).
- [7] D. Richardson and R. Hill, *J. Phys. C* **5**, 821 (1972).
- [8] D. Hsieh, D. Qian, L. Wray, Y. Xia, Y. S. Hor, R. J. Cava, and M. Z. Hasan, *Nature (London)* **452**, 970 (2008).
- [9] A. Narayan, D. Di Sante, S. Picozzi, and S. Sanvito, *Phys. Rev. Lett.* **113**, 256403 (2014).
- [10] T. C. V. Rauch, S. Achilles, J. Henk, and I. Mertig, *Phys. Rev. Lett.* **114**, 236805 (2015).
- [11] P. Dziawa, B. Kowalski, K. Dybko, R. Buczko, A. Szczerbakow, M. Szot, E. Łusakowska, T. Balasubramanian, B. M. Wojek, M. Berntsen *et al.*, *Nat. Mater.* **11**, 1023 (2012).
- [12] T.-R. Chang, S.-Y. Xu, G. Chang, C.-C. Lee, S.-M. Huang, B. Wang, G. Bian, H. Zheng, D. S. Sanchez, I. Belopolski *et al.*, *Nat. Commun.* **7**, 10639 (2016); I. Belopolski, D. S. Sanchez, Y. Ishida, X. Pan, P. Yu, S.-Y. Xu, G. Chang, T.-R. Chang, H. Zheng, N. Alidoust *et al.*, *Nat. Commun.* **7**, 13643 (2016).
- [13] H. Huang, J. Liu, and W. Duan, *Phys. Rev. B* **90**, 195105 (2014).
- [14] Z. Wang, Y. Sun, X.-Q. Chen, C. Franchini, G. Xu, H. Weng, X. Dai, and Z. Fang, *Phys. Rev. B* **85**, 195320 (2012); Z. K. Liu, B. Zhou, Y. Zhang *et al.*, *Science* **343**, 864 (2014); S.-Y. Xu, C. Liu, S. K. Kushwaha *et al.*, *Science* **347**, 294 (2015); J. Xiong, S. K. Kushwaha, T. Liang, J. W. Krizan, M. Hirschberger, W. Wang, R. J. Cava, and N. P. Ong, *Science* **350**, 413 (2015).
- [15] Z. Wang, H. Weng, Q. Wu, X. Dai, and Z. Fang, *Phys. Rev. B* **88**, 125427 (2013); M. Neupane, S.-Y. Xu, R. Sankar *et al.*, *Nat. Commun.* **5**, 3786 (2014); Z. K. Liu, J. Jiang, B. Zhou *et al.*, *Nat. Mater.* **13**, 677 (2014); S. Borisenko, Q. Gibson, D. Evtushinsky, V. Zabolotnyy, B. Buchner, and R. J. Cava, *Phys. Rev. Lett.* **113**, 027603 (2014).
- [16] S.-M. Huang, S.-Y. Xu, I. Belopolski, C.-C. Lee, G. Chang, B. Wang, N. Alidoust, G. Bian, M. Neupane, C. Zhang *et al.*, *Nat. Commun.* **6**, 7373 (2015); S.-Y. Xu,

- I. Belopolski, N. Alidoust, M. Neupane, G. Bian, C. Zhang, R. Sankar, G. Chang, Z. Yuan, C.-C. Lee *et al.*, *Science* **349**, 613 (2015); L. Yang, Z. Liu, Y. Sun, H. Peng, H. Yang, T. Zhang, B. Zhou, Y. Zhang, Y. Guo, M. Rahn *et al.*, *Nat. Phys.* **11**, 728 (2015).
- [17] H. Weng, C. Fang, Z. Fang, B. A. Bernevig, and X. Dai, *Phys. Rev. X* **5**, 011029 (2015); B. Q. Lv, H. M. Weng, B. B. Fu, X. P. Wang, H. Miao, J. Ma, P. Richard, X. C. Huang, L. X. Zhao, G. F. Chen, Z. Fang, X. Dai, T. Qian, and H. Ding, *Phys. Rev. X* **5**, 031013 (2015).
- [18] H. Yang, J. Yu, S. S. P. Parkin, C. Felser, C.-X. Liu, and B. Yan, *Phys. Rev. Lett.* **119**, 136401 (2017).
- [19] Z. Wang, M. G. Vergniory, S. Kushwaha, M. Hirschberger, E. V. Chulkov, A. Ernst, N. P. Ong, R. J. Cava, and B. A. Bernevig, *Phys. Rev. Lett.* **117**, 236401 (2016).
- [20] H. Weng, C. Fang, Z. Fang, and X. Dai, *Phys. Rev. B* **93**, 241202 (2016).
- [21] Z. Zhu, G. W. Winkler, Q. S. Wu, J. Li, and A. A. Soluyanov, *Phys. Rev. X* **6**, 031003 (2016).
- [22] B. Lv, Z.-L. Feng, Q.-N. Xu, X. Gao, J.-Z. Ma, L.-Y. Kong, P. Richard, Y.-B. Huang, V. Strocov, C. Fang *et al.*, *Nature (London)* **546**, 627 (2017); J.-Z. Ma, J.-B. He, Y.-F. Xu, B.-Q. Lv, D. Chen, W.-L. Zhu, S. Zhang, L.-Y. Kong, X. Gao, L.-Y. Rong *et al.*, *Nat. Phys.*, DOI: 10.1038/s41567-017-0021-8 (2018).
- [23] Y. Zhou, P. Lu, Y. Du, X. Zhu, G. Zhang, R. Zhang, D. Shao, X. Chen, X. Wang, M. Tian, J. Sun, X. Wan, Z. Yang, W. Yang, Y. Zhang, and D. Xing, *Phys. Rev. Lett.* **117**, 146402 (2016).
- [24] Z. Guo, P. Lu, T. Chen, J. Wu, J. Sun, and D. Xing, *Sci. China Phys. Mech. Astron.* **61**, 038211 (2018).
- [25] H. Weng, C. Fang, Z. Fang, and X. Dai, *Phys. Rev. B* **94**, 165201 (2016).
- [26] J.-P. Sun, D. Zhang, and K. Chang, *Phys. Rev. B* **96**, 045121 (2017).
- [27] J. Cano, B. Bradlyn, Z. Wang, M. Hirschberger, N. P. Ong, and B. A. Bernevig, *Phys. Rev. B* **95**, 161306 (2017).
- [28] E. V. Gorbar, V. A. Miransky, and I. A. Shovkovy, *Phys. Rev. B* **88**, 165105 (2013).
- [29] G. Kresse and J. Furthmüller, *Comput. Mater. Sci.* **6**, 15 (1996).
- [30] See Supplemental Material at <http://link.aps.org/supplemental/10.1103/PhysRevLett.120.136403>, for more details about the computation, which includes Refs. [31–66].
- [31] J. P. Perdew, K. Burke, and M. Ernzerhof, *Phys. Rev. Lett.* **77**, 3865 (1996).
- [32] P. E. Blöchl, *Phys. Rev. B* **50**, 17953 (1994).
- [33] A. A. Mostofi, J. R. Yates, Y.-S. Lee, I. Souza, D. Vanderbilt, and N. Marzari, *Comput. Phys. Commun.* **178**, 685 (2008).
- [34] H. Huang, K.-H. Jin, and F. Liu, *Phys. Rev. B* **96**, 115106 (2017).
- [35] M. P. López Sancho, J. M. López Sancho, and J. Rubio, *J. Phys. F* **14**, 1205 (1984); **15**, 851 (1985).
- [36] Q. Wu, S. Zhang, H.-F. Song, M. Troyer, and A. A. Soluyanov, *Comput. Phys. Commun.* **224**, 405 (2018).
- [37] J. C. Slater, *J. Chem. Phys.* **41**, 3199 (1964).
- [38] E. Clementi, D. Raimondi, and W. Reinhardt, *J. Chem. Phys.* **47**, 1300 (1967).
- [39] P. Pyykkö and M. Atsumi, *Chem. Eur. J.* **15**, 186 (2009).
- [40] P. Pyykkö, S. Riedel, and M. Patzschke, *Chem. Eur. J.* **11**, 3511 (2005).
- [41] B. Cordero, V. Gómez, A. E. Platero-Prats, M. Revés, J. Echeverría, E. Cremades, F. Barragán, and S. Alvarez, *Dalton Trans.* **0**, 2832 (2008).
- [42] R. Dronskowski, S. Kikkawa, and A. Stein, *Handbook of Solid State Chemistry* (Wiley-VCH, Weinheim, Germany, 2017).
- [43] N. Welham, *J. Mater. Sci.* **34**, 21 (1999).
- [44] H. Jacobs and E. Von Pinkowski, *J. Less-Common Met.* **146**, 147 (1989).
- [45] P. Rauch and F. DiSalvo, *J. Solid State Chem.* **100**, 160 (1992).
- [46] H. Jacobs and B. Hellmann, *J. Alloy Compd.* **191**, 51 (1993).
- [47] I. Ohkubo and T. Mori, *Chem. Mater.* **27**, 7265 (2015).
- [48] V. Balbarin, R. Van Dover, and F. DiSalvo, *J. Phys. Chem. Solids* **57**, 1919 (1996).
- [49] A. Zakutayev, A. J. Allen, X. Zhang, J. Vidal, Z. Cui, S. Lany, M. Yang, F. J. DiSalvo, and D. S. Ginley, *Chem. Mater.* **26**, 4970 (2014).
- [50] U. Zachwieja and H. Jacobs, *Eur. J. Solid State Inorg. Chem.* **28**, 1055 (1991).
- [51] A. Miura, M. Lowe, B. M. Leonard, C. V. Subban, Y. Masubuchi, S. Kikkawa, R. Dronskowski, R. G. Hennig, H. D. Abruña, and F. J. DiSalvo, *J. Solid State Chem.* **184**, 7 (2011).
- [52] R. Niewa, D. Zherebtsov, W. Schnelle, and F. Wagner, *Inorg. Chem.* **43**, 6188 (2004).
- [53] A. Bowman and D. H. Gregory, *J. Alloy Compd.* **348**, 80 (2003).
- [54] X. Chen, H. A. Eick, and W. Lasocha, *J. Solid State Chem.* **138**, 297 (1998).
- [55] O. Seeger, M. Hofmann, J. Strähle, J. Laval, and B. Frit, *Z. Anorg. Allg. Chem.* **620**, 2008 (1994).
- [56] L. Cario, Z. A. Gál, T. P. Braun, F. J. DiSalvo, B. Blaschkowski, and H.-J. Meyer, *J. Solid State Chem.* **162**, 90 (2001).
- [57] X. Chen and H. Eick, *J. Solid State Chem.* **130**, 1 (1997).
- [58] X. Chen and H. Eick, *J. Solid State Chem.* **113**, 362 (1994).
- [59] X. Chen, D. Ward, and H. Eick, *J. Alloy Compd.* **206**, 129 (1994).
- [60] L. Yang, Z. Liu, Y. Sun, H. Peng, H. Yang, T. Zhang, B. Zhou, Y. Zhang, Y. Guo, M. Rahn *et al.*, *Nat. Phys.* **11**, 728 (2015).
- [61] Q.-Y. Wang, Z. Li, W.-H. Zhang, Z.-C. Zhang, J.-S. Zhang, W. Li, H. Ding, Y.-B. Ou, P. Deng, K. Chang *et al.*, *Chin. Phys. Lett.* **29**, 037402 (2012).
- [62] S. Tan, Y. Zhang, M. Xia, Z. Ye, F. Chen, X. Xie, R. Peng, D. Xu, Q. Fan, H. Xu *et al.*, *Nat. Mater.* **12**, 634 (2013).
- [63] N. H. Tu, Y. Tanabe, Y. Satake, K. K. Huynh, P. H. Le, S. Y. Matsushita, and K. Tanigaki, *Nano Lett.* **17**, 2354 (2017).
- [64] C. L. Kane and E. J. Mele, *Phys. Rev. Lett.* **95**, 146802 (2005).
- [65] H. Huang, Z. Wang, N. Luo, Z. Liu, R. Lü, J. Wu, and W. Duan, *Phys. Rev. B* **92**, 075138 (2015).
- [66] T. Brokamp and H. Jacobs, *J. Alloy Compd.* **183**, 325 (1992).
- [67] G. Brauer, E. Mohr, A. Neuhaus, and A. Skokan, *Monatsh. Chem.* **103**, 794 (1972).

- [68] R. Niewa, D. Zharebtsov, W. Schnelle, and F. Wagner, *Inorg. Chem.* **43**, 6188 (2004).
- [69] Y. Li, P. Chen, G. Zhou, J. Li, J. Wu, B.-L. Gu, S. B. Zhang, and W. Duan, *Phys. Rev. Lett.* **109**, 206802 (2012).
- [70] S. Adachi, *Properties of Semiconductor Alloys: Group-IV, III-V and II-VI Semiconductors*, Vol. 28 (Wiley, New York, 2009).
- [71] J. Wang, X. Sui, W. Shi, J. Pan, S. Zhang, F. Liu, S.-H. Wei, Q. Yan, and B. Huang, *Phys. Rev. Lett.* **119**, 256402 (2017).
- [72] H. Störmer, R. Dingle, A. Gossard, W. Wiegmann, and M. Sturge, *Solid State Commun.* **29**, 705 (1979).
- [73] R. Dingle, H. Störmer, A. Gossard, and W. Wiegmann, *Appl. Phys. Lett.* **33**, 665 (1978).
- [74] H. M. Ng, D. Doppalapudi, D. Korakakis, R. Singh, and T. D. Moustakas, *J. Cryst. Growth* **189**, 349 (1998).
- [75] S. V. Novikov, A. Kent, and C. Foxon, *Prog. Cryst. Growth Charact. Mater.* **63**, 25 (2017).
- [76] J. Zhang, C.-Z. Chang, Z. Zhang, J. Wen, X. Feng, K. Li, M. Liu, K. He, L. Wang, X. Chen *et al.*, *Nat. Commun.* **2**, 574 (2011).
- [77] G. L. Bir and G. E. Pikus, *Symmetry and Strain-Induced Effects in Semiconductors* (Wiley, New York, 1974).
- [78] N. Marzari and D. Vanderbilt, *Phys. Rev. B* **56**, 12847 (1997); I. Souza, N. Marzari, and D. Vanderbilt, *Phys. Rev. B* **65**, 035109 (2001).
- [79] A. A. Soluyanov and D. Vanderbilt, *Phys. Rev. B* **83**, 235401 (2011).
- [80] I. Zeljkovic, Y. Okada, C.-Y. Huang, R. Sankar, D. Walkup, W. Zhou, M. Serbyn, F. Chou, W.-F. Tsai, H. Lin *et al.*, *Nat. Phys.* **10**, 572 (2014).
- [81] S. Jeon, B. B. Zhou, A. Gyenis, B. E. Feldman, I. Kimchi, A. C. Potter, Q. D. Gibson, R. J. Cava, A. Vishwanath, and A. Yazdani, *Nat. Mater.* **13**, 851 (2014).
- [82] H. Inoue, A. Gyenis, Z. Wang, J. Li, S. W. Oh, S. Jiang, N. Ni, B. A. Bernevig, and A. Yazdani, *Science* **351**, 1184 (2016); R. Batabyal, N. Morali, N. Avraham, Y. Sun, M. Schmidt, C. Felser, A. Stern, B. Yan, and H. Beidenkopf, *Sci. Adv.* **2**, e1600709 (2016); H. Zheng, S.-Y. Xu, G. Bian, C. Guo, G. Chang, D. S. Sanchez, I. Belopolski, C.-C. Lee, S.-M. Huang, X. Zhang *et al.*, *ACS Nano* **10**, 1378 (2016).
- [83] G. Chang, S.-Y. Xu, H. Zheng, C.-C. Lee, S.-M. Huang, I. Belopolski, D. S. Sanchez, G. Bian, N. Alidoust, T.-R. Chang, C.-H. Hsu, H.-T. Jeng, A. Bansil, H. Lin, and M. Z. Hasan, *Phys. Rev. Lett.* **116**, 066601 (2016).
- [84] H. Zheng, G. Chang, S.-M. Huang, C. Guo, X. Zhang, S. Zhang, J. Yin, S.-Y. Xu, I. Belopolski, N. Alidoust, D. S. Sanchez, G. Bian, T.-R. Chang, T. Neupert, H.-T. Jeng, S. Jia, H. Lin, and M. Z. Hasan, *Phys. Rev. Lett.* **119**, 196403 (2017).
- [85] A. Pariari and P. Mandal, *Sci. Rep.* **7**, 40327 (2017).
- [86] S. S. Hosmani, P. Kuppasami, R. K. Goyal *et al.*, *An Introduction to Surface Alloying of Metals* (Springer, New York, 2014).
- [87] A. Schmid, N. Bartelt, and R. Hwang, *Science* **290**, 1561 (2000).
- [88] J. Lu, K. Zhang, X. F. Liu, H. Zhang, T. C. Sum, A. H. C. Neto, and K. P. Loh, *Nat. Commun.* **4**, 2681 (2013).